Strain-Gage Methods for Measuring the Opening-Mode Stress-Intensity Factor, K_I

by J.W. Dally and R.J. Sanford

ABSTRACT—Measurements of strain near a crack tip with electrical-resistance strain gages do not usually provide a reliable measure of K_I because of local yielding, three-dimensional effects and limited regions for strain-gage placement. This paper develops expressions for the strains in a valid region removed from the crack tip, and indicates procedures for locating and orienting the gages to accurately determine K_I from one or more strain-gage readings.

Introduction

Although Irwin[1] first suggested the use of strain gages to determine the stress-intensity factor near the tip of a crack in 1957, little progress has been made in implementing this suggestion. The primary reason for the delay in the development of a suitable method involves the finite size of the strain gage. Questions arise regarding the effects of the strain gradients on the gage output, the magnitude of the strains to be measured if the gage is placed in close proximity to the crack tip, and the relative size of the gage compared to the size of the near-field region. A secondary reason for the delay is the availability of other experimental methods for determining the stress-intensity factor. Kobayashi[2] has described methods based on compliance measurements and photoelasticity. In addition Mannog[3] and Theocaris[4] have demonstrated the application of the method of caustics in a wide range of plane bodies containing cracks. Finally, Barker *et al.*[5] have shown an accurate numerical technique for determining the stress-intensity factor from full-field displacement data which can be obtained with either moiré or speckle photography.

This paper demonstrates that strain gages can be effectively employed to measure the stress-intensity factor. The application considered here is the determination of the opening-mode stress-intensity factor K_I in a plane body with a through crack.

The area adjacent to the crack tip is divided into three regions as shown in Fig. 1. The innermost region close to the crack tip, region I, is not a valid region for data acquisition because of nonlinearities caused by yielding or ambiguities concerning whether the stress state is plane stress or plane strain. The intermediate region, region II, is a valid area where the strain field can be represented within a specified accuracy by a multiparameter theory containing K_I and coefficients of higher order terms as unknowns. Region III, the outermost region, represents the far field where the truncated series describing the strain field is not sufficiently accurate. The boundary between region II and region III will depend upon the accuracy specified and the number of terms retained in the multiparameter theory. The area of region II is sufficiently large to accommodate common electrical-resistance strain gages.

The error due to strain gradient is first minimized by placing the strain gages sufficiently far from the crack tip, and is then eliminated by a simple integration procedure. The influence of the strain gradient in the θ direction is not treated because it is no larger than that normally encountered in strain-gage applications where the strain field varies as a trigonometric function of θ.

Multiparameter Representation of the Strain Field

Sanford[6] has shown that the Westergaard[7] equations should be generalized to solve fracture-mechanics problems where the stress field in the local neighborhood of the crack tip is influenced by the proximity of boundaries and points of load application. The stresses expressed in this generalized form are given by

$$\begin{aligned} \sigma_{xx} &= ReZ - yImZ' - yImY' + 2ReY \\ \sigma_{yy} &= ReZ + yImZ' + yImY' \\ \tau_{xy} &= -yReZ' - yReY' - ImY \end{aligned} \tag{1}$$

where, for a single-ended crack, the stress functions Z and Y can be represented by

$$\begin{aligned} Z(z) &= \sum_{n=0}^{N} A_n z^{n-1/2} \\ Y(z) &= \sum_{m=0}^{M} B_m z^m \end{aligned} \tag{2}$$

J.W. Dally (SEM Fellow) and R.J. Sanford (SEM Fellow) are Professors, University of Maryland, Department of Mechanical Engineering, College Park, MD 20742.

Original manuscript submitted: February 6, 1986. Final manuscript received: March 11, 1987.

where

$$z = x + iy \tag{3}$$

with the coordinate system defined in Fig. 2. By substituting eqs (1) into the plane stress-strain relations:

$$\epsilon_{xx} = \frac{1}{E}[\sigma_{xx} - \nu\sigma_{yy}]$$

$$\epsilon_{yy} = \frac{1}{E}[\sigma_{yy} - \nu\sigma_{xx}] \tag{4}$$

$$\gamma_{xy} = \frac{1}{\mu}\tau_{xy}$$

one obtains the following generalized equations for the strain field.

$$E\epsilon_{xx} = (1-\nu)ReZ - (1+\nu)yImZ' - (1+\nu)yImY' + 2ReY$$

$$E\epsilon_{yy} = (1-\nu)ReZ + (1+\nu)yImZ' + (1+\nu)yImY' - 2\nu ReY \tag{5}$$

$$\mu\gamma_{xy} = -yReZ' - yReY' - ImY$$

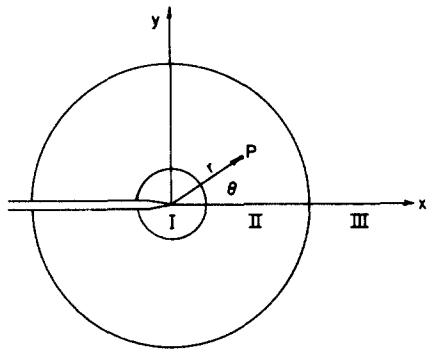

Fig. 1—Schematic illustration of the three regions associated with the near field for a compact-tension specimen at $a/W = 0.5$

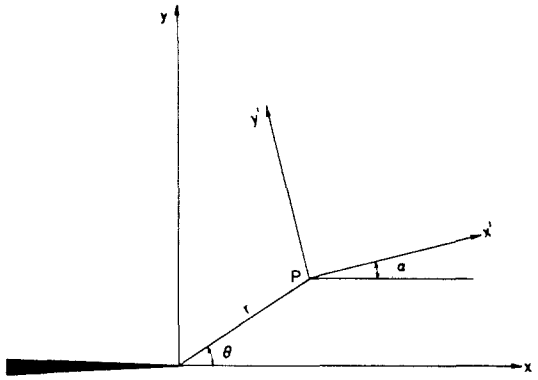

Fig. 2—Definition of coordinate systems Oxy and Px'y'

The strain field can be expressed exactly by using the infinite series representation of the stress functions Z and Y given in eq (2). This exact approach cannot, however, be utilized in practice due to the infinite number of unknown coefficients A_n and B_m. It is necessary to truncate the series and to accept a specified error in the representation of the strain field. In this paper, a four-term representation is described where the first two terms of each of the series for Z and Y have been retained. Of course, a higher-order theory could be developed, but the number of strain gages required to determine A_n and B_m would become prohitibively large.

Setting $n = 0,1$ and $m = 0,1$ gives

$$Z = A_0 r^{-1/2}[\cos(\theta/2) - i\sin(\theta/2)] + A_1 r^{1/2}[\cos(\theta/2) + i\sin(\theta/2)]$$

$$Y = B_0 + B_1 r[\cos\theta + i\sin\theta] \tag{6}$$

Substituting eqs (6) into eqs (5) gives

$$E\epsilon_{xx} = A_0 r^{-1/2}\cos(\theta/2)[(1-\nu) - (1+\nu)\sin(\theta/2)\sin(3\theta/2)] + 2B_0 + A_1 r^{1/2}\cos(\theta/2)[(1-\nu) + (1+\nu)\sin^2(\theta/2)] + 2B_1 r\cos\theta$$

$$E\epsilon_{yy} = A_0 r^{-1/2}\cos(\theta/2)[(1-\nu) + (1+\nu)\sin(\theta/2)\sin(3\theta/2)] - 2\nu B_0 + A_1 r^{1/2}\cos(\theta/2)[(1-\nu) - (1+\nu)\sin^2(\theta/2)] - 2\nu B_1 r\cos\theta$$

$$\mu\gamma_{xy} = (A_0/2)r^{-1/2}\sin\theta\cos(3\theta/2) - (A_1/2)r^{1/2}\sin\theta\cos(\theta/2) - 2B_1 r\sin\theta \tag{7}$$

This representation of the strain field could be employed with data from strain gages positioned at arbitrary points $[P_1(r_1,\theta_1), P_2(r_2,\theta_2), P_3(r_3,\theta_3)$ and $P_4(r_4,\theta_4)]$ all located in region II and oriented in either the x or y directions to obtain a solution for A_0 which is related to K_I by

$$K_I = \sqrt{2\pi}A_0 \tag{8}$$

However, it is advantageous to consider orientation of the strain gages at an arbitrary angle α, as illustrated in Fig. 2, to explore the possibility of eliminating some of the terms in the strain-field representation by gage positioning and orientation.

Four-Parameter Strain Field Relative to a Rotated Coordinate System

The strains relative to a rotated coordinate system (x', y') with its origin at an arbitrary point $P(r,\theta)$ as defined in Fig. 2 are determined from the first invariant of strain,

$$\epsilon_{x'x'} + \epsilon_{y'y'} = \epsilon_{xx} + \epsilon_{yy} \tag{9}$$

and the complex form of the strain-transformation equations,

$$\epsilon_{y'y'} - \epsilon_{x'x'} + i\gamma_{x'y'} = (\epsilon_{yy} - \epsilon_{xx} + i\gamma_{xy})e^{2i\alpha} \tag{10}$$

Substituting eq (5) into eq (10) leads to

$$2\mu\epsilon_{x'x'} = \frac{1-\nu}{1+\nu}(ReZ + ReY) -$$

$$(yImZ' + yImY' - ReY)\cos 2\alpha -$$

$$(yReZ' + ReY' + ImY)\sin 2\alpha$$

$$2\mu\epsilon_{y'y'} = \frac{1-\nu}{1+\nu}(ReZ + ReY) +$$

$$(yImZ' + yImY' - ReY)\cos 2\alpha +$$

$$(yReZ' + yReY' + ImY)\sin 2\alpha \qquad (11)$$

Again letting $n = 0,1$ and $m = 0,1$ in eq (2) and substituting the results for the truncated series into eq (11) yields

$$2\mu\epsilon_{x'x'} = A_0 r^{-1/2}[k\cos(\theta/2) - (1/2)\sin\theta\sin(3\theta/2)\cos 2\alpha$$

$$+ (1/2)\sin\theta\cos(3\theta/2)\sin 2\alpha] + B_0(k + \cos 2\alpha) +$$

$$A_1 r^{1/2}\cos(\theta/2)[k + \sin^2(\theta/2)\cos 2\alpha - (1/2)\sin\theta\sin 2\alpha]$$

$$+ B_1 r[(k + \cos 2\alpha)\cos\theta - 2\sin\theta\sin 2\alpha] \qquad (12)$$

$$\mu(\epsilon_{y'y'} - \epsilon_{x'x'}) = (A_0/2)r^{-1/2}\sin\theta[\sin(3\theta/2)\cos 2\alpha -$$

$$\cos(3\theta/2)\sin 2\alpha] -$$

$$B_0\cos 2\alpha + (A_1/2)r^{1/2}\sin\theta[\cos(\theta/2)\sin 2\alpha -$$

$$\sin(\theta/2)\cos 2\alpha] + B_1 r[2\sin\theta\sin 2\alpha - \cos\theta\cos 2\alpha] \qquad (13)$$

where

$$k = (1-\nu)/(1+\nu) \qquad (14)$$

Equation (12) gives the relations between K_I and the strain $\epsilon_{x'x'}$ measured with a single-element strain gage oriented at an angle α with respect to the P(x' y') coordinate system. Equation (13) gives the relation between K_I and the output of a rectangular rosette with the two elements connected to adjacent arms of a Wheatstone bridge. There are many options regarding gage positioning and orientation to simplify eqs (7), (12) and (13). However, before considering these options it is necessary to more closely examine region II and to determine its bounds, since it is essential that the gage position $P(r,\theta)$ be located within this region to avoid excessive errors.

Crack-Tip Regions

The size and shape of region II can be determined for say $\epsilon_{x'x'}$ by comparing the results of eq (12) with an exact solution of a representative fracture-mechanics problem. To illustrate this procedure, consider the compact-tension specimen with $a/W = 0.5$ subjected to pin loading. Chona *et al.*[8] have determined the coefficients A_0, A_1, A_2, B_0, B_1 and B_2 to obtain a six-parameter solution for the stress field which is considered to represent an exact solution over a region of some extent around the crack tip. Approximate values of the strains $\epsilon_{x'x'}$ for $\alpha = 60$ deg were determined from eq (12) over the field by using one or more of these coefficients. For example, a one-parameter representation of $\epsilon_{x'x'}$ utilizes A_0 with $A_1 = A_2 = B_0 = B_1 = B_2 = 0$; a two-parameter solution utilizes A_0 and B_0; a three-parameter solution utilizes A_0, B_0, and A_1; and finally a four-parameter solution contains A_0, B_0, A_1, and B_1.

A point by point comparison was made over the field to determine the difference between the exact (six coefficient) and approximate values of $\epsilon_{x'x'}$. A plotting routine was then used to provide maps of the area around the crack tip where the differences were within ± 2, ± 5, and ± 10 percent. The results obtained for the compact-tension specimen over a ± 0.25 W sized zone about the crack tip are shown in Fig. 3. An examination of these results shows two very clear trends. Firstly, the size of region II increases markedly as additional terms are added to the series representation of $\epsilon_{x'x'}$. Note that the second term (i.e., B_0) does not affect the size or shape of region II because of the choice of $\alpha = 60$ deg (for $\nu = \frac{1}{3}$) which eliminates this term in eq (12) for all values of r and θ. Secondly, the size of region II depends strongly on the accuracy required. However, in all cases considered, ± 2, ± 5 and ± 10-percent accuracies, the size of region II is large enough to accommodate several strain gages.

Region II has been divided into two parts in Fig. 3, namely IIa and IIb. Region IIb is a valid region from an accuracy viewpoint; however, the strain $\epsilon_{x'x'}$ in IIb will be quite low and is not a suitable area for strain-gage placement. The magnitude of the strain in IIa is much larger; gage placement should be restricted to this area.

The inner boundary of region II is determined by a circle of radius:

$$r = h/2 \qquad (15)$$

where h is the thickness of the plane body. Rosakis and Ravi-Chandra[9] have shown experimentally that the state of stress at the crack tip is three dimensional in region I and is not represented by either plane stress or plane strain. Plane-stress conditions exist only when $r > h/2$.

Strain-Gage Position and Orientation

There are many possible approaches to determining K_I by employing eqs (7), (12) and (13). Only three approaches will be described here to illustrate some of the procedures to be followed in reducing the theory to practice. These approaches include: (1) the single gage—three-parameter solution, (2) the two gage-four-parameter solution and (3) the rectangular rosette—two- or three-parameter solution with temperature compensation. Each of these three approaches is covered as individual cases below.

Case I: Single Gage—Three-Parameter Solution

Consider first eq (12) for $\epsilon_{x'x'}$ and note that the B_0 term can be eliminated if

$$\cos 2\alpha = -k = -(1-\nu)/(1+\nu) \qquad (16)$$

Next, set the coefficient of the A_1 term to zero.

$$k + \sin^2(\theta/2)\cos 2\alpha - (\tfrac{1}{2})\sin\theta\sin 2\alpha = 0$$

which can be satisfied if

$$\tan(\theta/2) = -\cot 2\alpha \qquad (17)$$

These results show that a single-element gage can be used to provide the data necessary for a three-parameter solu-

tion for K_I providing the angles α and θ are selected to satisfy eqs (16) and (17). These angles depend only on a Poisson's ratio, ν, of the specimen material as indicated in Table 1.

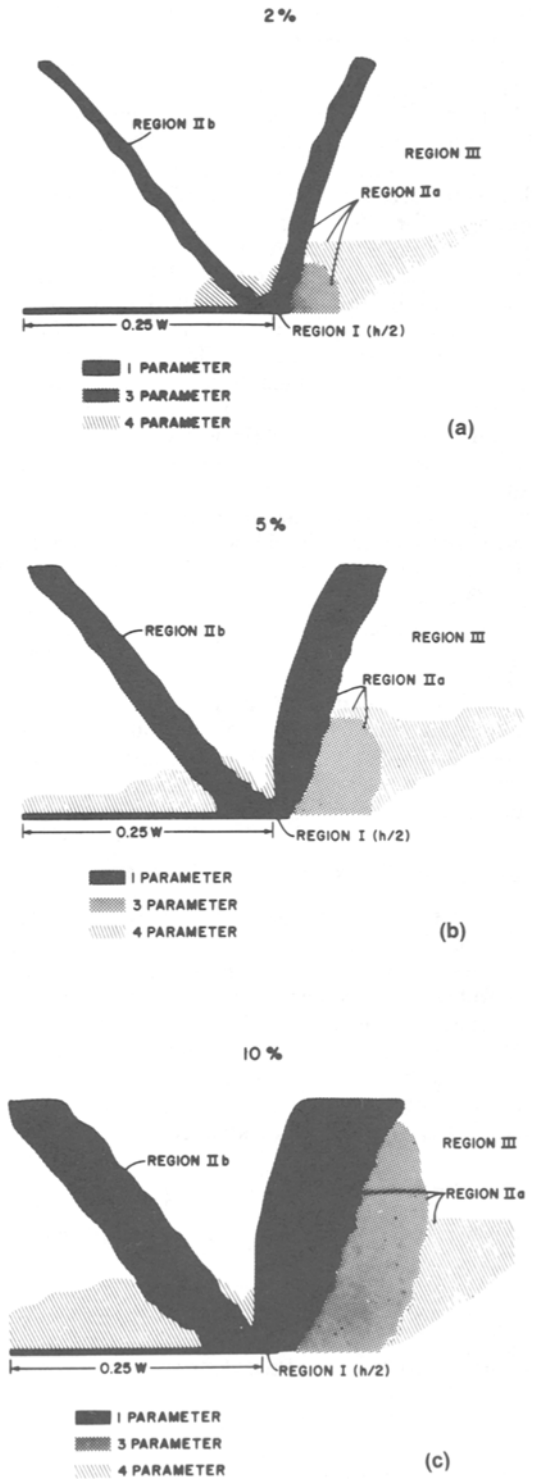

Fig. 3—Size of the valid region for $\epsilon_{x'x'}$ with $\alpha = 60$ deg and $\nu = 1/3$ as a function of the number of terms used in the series representation for a compact-tension specimen with $h = 0.250$ in. (6.3 mm). (a) Two-percent accuracy, (b) five-percent accuracy, (c) ten-percent accuracy

Take, for example, an aluminum specimen with $\nu = \frac{1}{3}$. Then $\alpha = \theta = 60$ deg, and the gage is placed at any point in region II along a 60-deg radial line drawn from the crack tip. For this example (i.e., $\nu = \frac{1}{3}$) eq (12) reduces to

$$2\mu\epsilon_{x'x'} = A_0 r^{-1/2} 3\sqrt{3}/8 \qquad (18)$$

Substituting eq (8) into eq (18) and solving for K_I gives

$$K_I = E\sqrt{(8/3)\pi r}\,\epsilon_{x'x'} \qquad (19)$$

Measuring the gage position r and recording the strain $\epsilon_{x'x'}$ from the single gage gives the data necessary to determine K_I with an accuracy consistent with the differences associated with region II.

Case II: Two Gages—Four-Parameter Solution

It is possible to obtain the data necessary to determine K_I from a four-parameter representation by using two strain gages, providing these gages are both placed in region II with the same value of θ and α as specified in Table 1. It is clear then that eq (12) subjected to the restrictions of eqs (16) and (17) reduces to

$$2\mu\epsilon_{x'x'} = A_0 r^{-1/2}[k\cos(\theta/2) + (k/2)\sin\theta\sin(3\theta/2) + (\tfrac{1}{2})\sin\theta\cos(3\theta/2)\sin 2\alpha] - 2B_1 r\sin\theta\sin 2\alpha \qquad (20)$$

The two strain-gage readings $(\epsilon_{x'x'})_A$ and $(\epsilon_{x'x'})_B$ and their respective positions r_A, r_B and $\theta_A = \theta_B$ can be used to solve eq (20) for A_0 and B_1. To demonstrate this fact and to show the simplicity of this approach, consider again the aluminum specimen with $\nu = \frac{1}{3}$ and $\alpha_A = \alpha_B = \theta_A = \theta_B = 60$ deg. With these substitutions, eq (20) reduces to

$$E\epsilon_{x'x'} = (\sqrt{3}/2)A_0 r^{-1/2} - 2B_1 r \qquad (21)$$

Solving eq (21) for A_0 or K_I using data from gages A and B gives

$$K_I = E\sqrt{(8/3)\pi r_A r_B}\left[\frac{(\epsilon_{x'x'})_A r_B - (\epsilon_{x'x'})_B r_A}{r_B^{3/2} - r_A^{3/2}}\right] \qquad (22)$$

If $r_B = q r_A$, then eq (22) becomes

$$K_I = E\sqrt{(8/3)\pi r_A}\,[q(\epsilon_{x'x'})_A - (\epsilon_{x'x'})_B]\left(\frac{\sqrt{q}}{q^{3/2}-1}\right) \qquad (23)$$

The four-parameter solution should be employed with bodies where the crack tip is relatively close to the boundaries and/or loading points, and the strain field requires the fourth term in the series for a more accurate representation.

TABLE 1—ANGLES α AND θ AS A FUNCTION OF POISSON'S RATIO, ν

ν	θ (deg)	α (deg)
0.250	73.74	63.43
0.300	65.16	61.29
0.333	60.00	60.00
0.400	50.76	57.69
0.500	38.97	54.74

Case III: Rectangular Rosette

In some applications in materials testing, the fracture specimen is subjected to a temperature gradient and temperature compensation is important. In these instances it is advisable to employ a stacked rectangular rosette and to place the two gages in adjacent arms of a Wheatstone bridge to achieve temperature compensation. The output from the bridge gives the measurement of $\epsilon_{y'y'} - \epsilon_{x'x'}$ which is shown in eq (13). It is evident from this equation that the coefficient of the B_0 term will vanish if

$$\cos 2\alpha = 0 \quad \text{or} \quad \alpha = \pi/4 \tag{24}$$

With this restriction eq (13) reduces to

$$\mu(\epsilon_{y'y'} - \epsilon_{x'x'}) = -(A_0/2)r^{-1/2}\sin\theta\cos(3\theta/2) + (A_1/2)r^{1/2}\sin\theta\cos(\theta/2) + 2B_1 r\sin\theta \tag{25}$$

Examination of eq (25) shows that θ cannot be selected to eliminate the coefficients of A_1 or B_1 without eliminating the coefficient of A_0. This fact indicates that a single two-element rectangular rosette can only be employed in a two-parameter solution for K_I.

To obtain the two-parameter solution, let $\theta = \pi/2$ and let $A_1 = B_1 = 0$. Equation (25) then gives

$$K_I = \frac{2E}{1+\nu}(\epsilon_{y'y'} - \epsilon_{x'x'})\sqrt{\pi r} \tag{26}$$

It is possible to obtain a three-parameter solution for K_I if the value of A_1/A_0 is known or can be estimated. Again, for $\theta = \frac{\pi}{2}$ with $\alpha = \frac{\pi}{4}$ and $B_1 = 0$, eq (25) becomes

$$\mu(\epsilon_{y'y'} - \epsilon_{x'x'}) = (\sqrt{2}/4)A_0 r^{-1/2}[1 + (A_1/A_0)r] \tag{27}$$

which can be rewritten as

$$K_I = K_{I\,app}/[1 + (A_1/A_0)r] \tag{28}$$

where $K_{I\,app}$ is obtained from eq (26).

An estimate of (A_1/A_0) can be obtained if two or more rosettes are positioned along the line $\theta = \pi/2$. For small values of r, eq (28) can be approximated by

$$K_I \approx K_{I\,app}[1 - (A_1/A_0)r + \ldots.] \tag{29}$$

From the measured strain readings a plot of $K_{I\,app}$ versus position is constructed and the limiting value of the slope taken, as illustrated in Fig. 4. From the plotted data, K_I = intercept, and $(A_1/A_0)K_I \approx$ limiting slope.

Strain-Gradient Effects

The error due to strain-gradient effects can be shown by considering a single-element strain-gage positioned in region IIa with $\alpha = \theta = 60$ deg. The gage senses the strain $\epsilon_{x'x'}$ given in eq (18). Its signal represents the average strain over its length which is given by

$$\epsilon_{x'x'}\Big|_{ave} = \frac{k_i}{r_0 - r_i}\int_{r_i}^{r_0} r^{-1/2}dr = 2k_i/(r_0^{1/2} + r_i^{1/2}) \tag{30}$$

where $k_i = K_I/E\sqrt{(8/3)\pi}$ and r_0 and r_i are positions of the active gage element as shown in Fig. 5. The gage output

$$\epsilon_{x'x'}\Big|_{ave}$$

corresponds to the true strain $\epsilon_{x'x'}$ at a specific point r_t along the gage length. It is evident from eqs (18) and (30) that

$$r_t = (r_0^{1/2} + r_i^{1/2})^2/4 \tag{31}$$

The position of the geometric center r_c of the gage is

$$r_c = (r_0 + r_i)/2 \tag{32}$$

Defining Δr as the distance between the geometric center of the gage, r_c, and the true strain point, r_t, gives

$$\Delta r = r_c - r_t = (r_0 - 2r_0^{1/2}r_i^{1/2} + r_i)/4 \tag{33}$$

Noting that the gage length L is

$$L = r_0 - r_i \tag{34}$$

and combining eqs (32), (33) and (34), it is evident that

$$(\Delta r/r_c) = [1 - \sqrt{1 - (L/2r_c)^2}]/2 \tag{35}$$

where $r_c > (L/2)$ to avoid placing the gage over the crack tip. The results from eq (35) which show $(\Delta r/r_c)$ as a

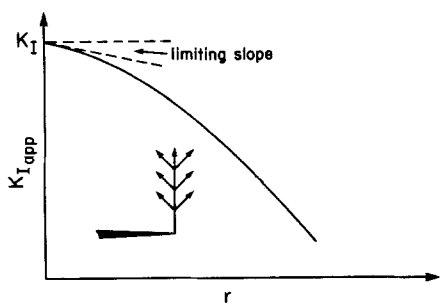

Fig. 4—Rosette data for $K_{I\,app}$ as a function of position r showing the limiting slope, and intercept K_I

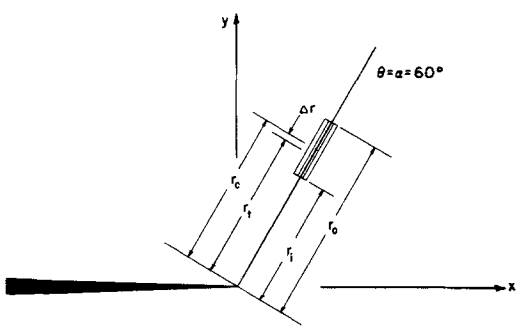

Fig. 5—Definition of radii associated with gage placement near a crack tip

function of (r_c/L) are presented in Fig. 6. The strain-gradient effect is a maximum $(\Delta r/r_c = 0.5)$ when the gage is placed as close as possible to the crack tip with $r_c = -L/2$. This placement should be avoided in any event since all or part of the gage is in region I where the plane stress analysis presented here is not valid. For gages placed in region IIa, r_c/L will probably exceed two and the effect of the strain gradient is much smaller. If a correction is required, r_t is determined from eq (31). This value is used in eq (19) to determine K_I. In many applications a correction may not be required. For example consider a gage with $L = 0.030$ in. (0.76 mm) positioned at $r_c = 5L$, and note from Fig. 6 that $\Delta r/r_c = 0.0025$. The correction $\Delta r = 0.000375$ in. (0.0095 mm) is much less than the accuracy which can be achieved in measuring r_c.

Experimental Verification

A compact-tension specimen with $W = 12$ in. (305 mm) was fabricated from a 0.250-in. (6.35-mm) thick plate of aluminum 6061T6 with a machined crack of length $a/W = 0.5$ to verify the theory. Three single-element strain gages with an active grid 0.030 × 0.030 in. (0.76 × 0.76 mm) were positioned along the line $\alpha = \theta = 60$ deg at $r = 0.192$, 0.483 and 0.783 in. (4.88, 12.27 and 19.89 mm). Three two-element rectangular rosettes were positioned along the line $\theta = 90$ deg, all with $\alpha = 45$ deg and $r = 0.233$, 0.500 and 0.767 in. (5.92, 12.70, 19.48 mm). The specimen was loaded in 200-lb (890-N) increments. The strains were measured at each load increment. The strains $\epsilon_{x'x'}$ and $\epsilon_{y'y'} - \epsilon_{x'x'}$ for the single element and rosettes are given in Table 2 for a load of 2000 lb (8900 N).

The strains were then substituted into eq (19) or eq (28) and the experimental values of K_I determined. For the rosette calculations a value of $(A_1/A_0) = -1/3$ was used.[8] These experimental values were compared to a theoretical value of K_I which was computed from the ASTM formula.[10] Comparisons of the experimental and theoretical results shown in Table 2 indicate that the values of K_I determined with single-element strain gages were consistently less than the theoretical value with differences ranging from 4.7 percent to 12.0 percent. It should also be noted that the largest difference occurred with data from gages close to the tip of the machined crack.

There are two reasons which lead to this difference. Firstly, the crack geometry (its width and sharpness) deviated from the theoretical model and these differences affected the strain field with the largest differences occurring at gage positions close to the crack tip. Secondly, the very large strains predicted by fracture-mechanics theory as r approaches zero cannot be achieved; the material very near the crack tip yields and the stress is redistributed to maintain equilibrium.

To account for the effects of the redistribution of the stress on the strain near the crack tip, Irwin's method of shifting the elastic field by the plastic-zone radius, r_y, to account for the finite stress at the crack tip was used. The r_y correction has two effects on the calculation of K_I from strain-gage data. First, the angle, θ, no longer has the required value to satisfy eq (17). Second, the radius changes. Both of these effects are illustrated in Fig. 7. From the figure it can be shown that

$$r' = r\left[1 - 2\left(\frac{r_y}{r}\right)\cos\theta + \left(\frac{r_y}{r}\right)^2\right]^{1/2} \qquad (36a)$$

TABLE 2—STRAIN-GAGE POSITIONS, STRAIN MEASUREMENT, K_I RESULTS AND THE DIFFERENCE BETWEEN THEORETICAL AND EXPERIMENTAL RESULTS FOR 2000-lb (8900-N) LOAD

Gage No.	r in. (mm)	$\epsilon_{x'x'}$ ($\times 10^{-6}$)	K_I ksi$\sqrt{\text{in.}}$ (MPa$\sqrt{\text{m}}$)	Difference* percent
1	0.192 (4.88)	1533	19.8 (21.8)	−12.0
2	0.483 (12.27)	1038	21.3 (23.4)	−4.7
3	0.783 (19.89)	813	21.2 (23.3)	−5.0
Rosette No.		$\epsilon_{y'y'} - \epsilon_{x'x'}$ ($\times 10^{-6}$)	K_I ksi$\sqrt{\text{in.}}$ (MPa$\sqrt{\text{m}}$)	
4	0.233 (5.92)	1555	22.1 (24.3)	−0.9
5	0.500 (12.70)	1015	23.4 (25.7)	4.9
6	0.767 (19.48)	727	23.2 (25.5)	4.0

*$K_I = 22.3$ ksi$\sqrt{\text{in.}}$ (24.5 MPa$\sqrt{\text{m}}$) ASTM formula

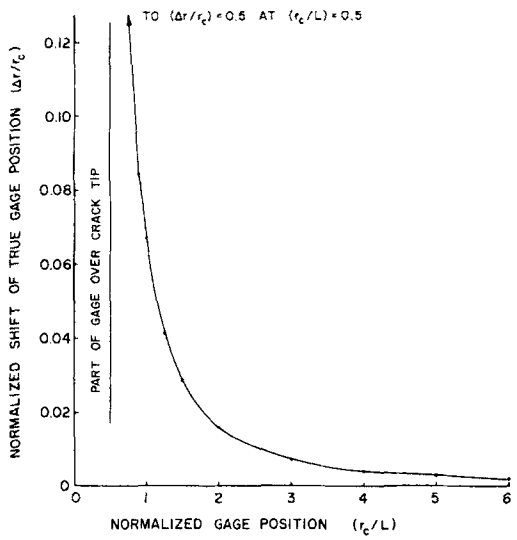

Fig. 6—Normalized shift of true gage position $\Delta r/r_c$ as a function of normalized position r_c/L

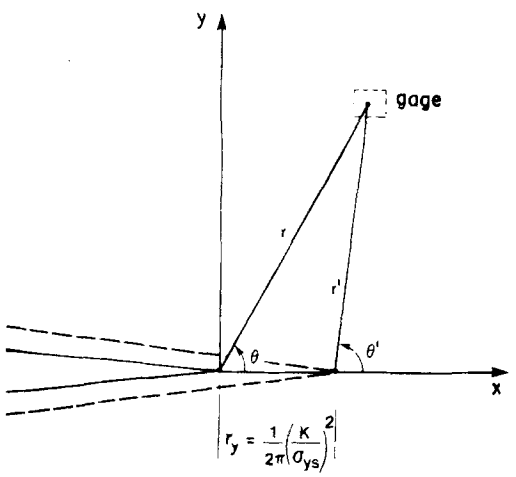

Fig. 7—Effect of the plastic-zone correction on the coordinates of a single-element strain gage

and

$$\theta' = \tan^{-1}\left[\frac{\text{Sin } \theta}{(\cos\theta - \frac{r_y}{r})}\right] \quad (36b)$$

For single-element gages initially satisfying eqs (16) and (17), eq (12) can be expressed in the form

$$2\mu\epsilon_{x'x'} \approx \frac{A_0}{(r)^{1/2}} f(\theta) \quad (37)$$

where $f(\theta)$ is obtained from the leading term in eq (12). When the plastic-zone corrected coordinates r', θ' are used, eq (12) becomes

$$2\mu\epsilon_{x'x'} \approx \frac{A_0{}^c}{(r')^{1/2}} f(\theta') \quad (38)$$

where $A_0{}^c$ is the plastic-zone corrected estimate of A_0. Equating eqs (37) and (38) yields

$$A_0{}^c = A_0 \left(\frac{r'}{r}\right)^{1/2} \frac{f(\theta)}{f(\theta')} \quad (39)$$

The combined effects of these errors can, to the first order, be expressed as a function of r_y/r as shown in Fig. 8 for various values of Poisson's ratio. There is an additional correction due to the A_1 term in eq (12); however, for single-element gages approximately satisfying eq (17), the contribution due to this term is less than one percent even for the closest gage. The experimental results for single-element gages, corrected for finite-stress effects, are given in Table 3.

TABLE 3—SINGLE-GAGE RESULTS CORRECTED FOR FINITE CRACK-TIP STRESSES

Gage No.	K_I-Uncorrected ksi$\sqrt{\text{in.}}$ (MPa$\sqrt{\text{m}}$)	K_I-Corrected ksi$\sqrt{\text{in.}}$ (MPa$\sqrt{\text{m}}$)	Error* percent
1	19.8 (21.7)	23.8 (26.1)	6.5
2	21.3 (23.4)	22.7 (24.9)	1.8
3	21.2 (23.3)	22.0 (24.2)	−1.5

*Based on a theoretical value of K_I = 22.3 ksi$\sqrt{\text{in.}}$ (24.5 MPa$\sqrt{\text{m}}$), compared to K_I corrected, as determined from strain-gage measurements

For the case of rosette gages the correction for finite stresses at the crack tip cannot be expressed solely in terms of the ratio r_y/r. Since there is no angle for which the A_1 contribution to the K measurement can be neglected, the influence of this term must be included in the finite stress corrections. An analysis of eq (13) reveals that the correction factor is highly sensitive to estimates of A_1 and r_y/r. As a result, the correction of rosette results is not practical.

Summary

A general method for determining K_I with common commercially available strain gages has been developed in terms of the generalized Westergaard stress functions. A four-parameter solution for K_I was derived from these stress functions to give an experimental approach for measuring K_I with a small number of strain gages.

The area adjacent to the crack tip was divided into three regions. Region I very near the crack tip is invalid because of three-dimensional effects. Region III far from the crack tip is invalid because the truncated series solution does not adequately describe the strain field. Region II located between regions I and III is a valid area where the truncated-series solution represents the strain field to a specified accuracy. The size and shape of region II is presented for the compact-tension geometry. Region II was subdivided into regions IIa and IIb. Region IIb was discarded because the strains in this area are too low for accurate measurement.

Three specific cases are considered in reducing the four-parameter theory to a simple and practical approach. It is shown that a single gage element with proper placement and orientation can be used to provide measurement of K_I while accounting for the effect of the first two non-singular terms. Two in-line single-element gages provide the data necessary to measure K_I with a four-parameter theory. The use of rosettes for the measurement of K_I is inherently less efficient since more gages are required; however, temperature compensation can be achieved on fracture specimens where thermal gradients are required on the specimen. The use of a single rosette gives the

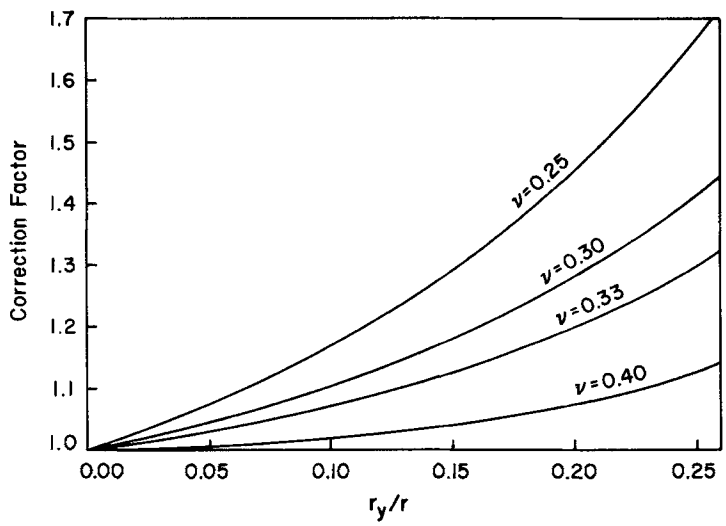

Fig. 8—Finite crack-tip stress correction for single-element gages as a function of r_y/r for various values of Poisson's ratio

data necessary for a two-parameter determination of K_I. The use of two or more rosettes permits a three-parameter determination. A graphical technique is introduced for the rosette approach which permits the experimentalist to determine the need for a higher-order theory. This technique is also applicable for single-element gages if they are placed along a radial line with θ constant.

The effect of strain gradients is considered. A method is shown to locate the true position of the gage, eliminating error due to the strain gradient in the radial direction. It is also shown that the difference between the geometric center of the gage and the true strain position becomes small as r_c/L increases.

Finally, experiments conducted to verify the theory show that K_I determined with single-element strain gages consistently underestimates the theoretical value, with the gages located close to the crack tip exhibiting the largest difference (12 percent). It is believed that these differences are due mainly to the crack-tip geometry of the model and localized yielding at the crack tip. A correction method has been developed to adjust the results for the effects of finite stresses at the crack tip. The results for K_I after correction show differences ranging from -1.5 to 6.5 percent between the theoretical and experimental values. Similarly, the results obtained with rosette gages show acceptable agreement with the theory, i.e., within five percent.

Acknowledgments

The authors are grateful to Mr. Ravi Chona for the computer run necessary to generate Fig. 3 and to Mr. John R. Berger for his assistance in conducting the experiments. Research funding for this project was provided by Martin Marietta Energy Systems (ORNL), Dr. C.E. Pugh, program manager and the National Science Foundation under grant No. MSM-85-13037, Dr. S. Jahanmir, program director.

References

1. *Irwin, G.R., "Analysis of Stresses and Strains Near the End of a Crack Traversing a Plate," J. Appl. Mech.,* **24** *(3), (1957).*
2. *Experimental Techniques in Fracture Mechanics, ed. A.S. Kobayashi, SEM Monograph, Iowa State University Press (1973).*
3. *Mannog, P., "Schattenoptische Messung der Spezifischen Bruchenergie wahrend des Bruchvorgangs bei Plexiglas," Proc. Int. Conf. on the Physics of Non-Crystalline Solids, Delft, The Netherlands, 481-490 (1964).*
4. *Theocaris, P.S., "Local Yielding Around A Crack Tip in Plexiglas," J. Appl. Mech.,* **37**, *409-415 (1970).*
5. *Barker, D.B., Sanford, R.J. and Chona, R., "Determining K and Related Stress-Field Parameters from Displacement Fields,"* EXPERIMENTAL MECHANICS, **25** *(4), 399-406 (1985).*
6. *Sanford, R.J., "A Critical Re-examination of the Westergaard Method for Solving Opening-Mode Crack Problems," Mech. Res. Comm.,* **6** *(5), (1979).*
7. *Westergaard, H.M., "Bearing Pressure and Cracks," J. Appl. Mech.,* **6** *(1939).*
8. *Chona, R., Irwin, G.R. and Sanford, R.J., "Influence of Specimen Size and Shape on the Singularity-Dominated Zone," Fracture Mechanics: Fourteenth Symposium - Volume 1: Theory and Analysis, ASTM STP 791, eds. J.C. Lewis and G. Sines, Amer. Soc. Test. and Mat., I-3-I-23 (1983).*
9. *Rosakis, A.J. and Ravi Chandra, K., "On Crack Tip Stress States and Experimental Evaluation of Three-Dimensional Effects," Cal. Inst. of Tech. Rep., FM-84-2 (March 1984).*
10. *ASTM-Standard E399-83, "Standard Test Methods for Plane-Strain Fracture Toughness of Metallic Materials," 1983 Annual Book of ASTM Standards,* **03.01**, *ASTM (1983).*
11. *Irwin, G.R., "Plastic Zone Near a Crack and Fracture Toughness," Proc. 7th Sagamore Conf., IV-63 (1960).*

An Experimental Investigation of How Accurate Simply Supported Boundary Conditions Can Be Achieved in Compression Testing Panels

Paper by Jose Maria Minguez appears in the September 1986 issue of EXPERIMENTAL MECHANICS, pages 238-244

Discussion

by Fok Wing Chau

The paper discusses the design and construction of a test rig with the aim of simulating a simply supported boundary condition for a panel under edge compression for both loaded and unloaded edges. Results of the experiments are interpreted by Southwell plot to verify the critical load of the plate when compared with the theoretical prediction. It is concluded that the theoretical simply supported boundary condition has probably not been fully achieved.

Fok Wing Chau (SEM Member) is Senior Lecturer, Nanyang Technological Institute, School of Mechanical and Production Engineering, Nanyang Avenue, Singapore 2263.